IEEE Access
Multidisciplinary | Rapid Review | Open Access Journal

Received 14 June 2024, accepted 26 June 2024, date of publication 1 July 2024, date of current version 9 July 2024.

Digital Object Identifier 10.1109/ACCESS.2024.3421353

RESEARCH ARTICLE

Secured NOMA Full-Duplex Transmission With Energy Harvesting

TOI LE-THANH[1] AND KHUONG HO-VAN[2,3], (Member, IEEE)
[1]Faculty of Electrical and Electronics Technology, HCMC University of Industry and Trade, Ho Chi Minh City 700000, Vietnam
[2]Department of Telecommunications Engineering, Ho Chi Minh City University of Technology, Ho Chi Minh City 700000, Vietnam
[3]Vietnam National University Ho Chi Minh City, Ho Chi Minh City 700000, Vietnam

Corresponding author: Khuong Ho-Van (hvkhuong@hcmut.edu.vn)

ABSTRACT Nonorthogonal multiple access (NOMA) enhances spectral efficiency by enabling manifold devices to utilize the same frequency-time resource through nonorthogonal signal superposition. In addition, full-duplex (FD) transmission allows concurrent reception and transmission on the same frequency range, further improving spectral efficiency. Moreover, nearby wireless energy sources are utilized to enhance energy efficiency. Nonetheless, several challenges are inherent in NOMA FD transmission with energy harvesting (NOFE), including information security concerns and practical imperfections such as channel state information imperfection (CSIi), hardware impairment (HWi), and successive interference cancellation imperfection (SICi). The paper first proposes a solution to address these challenges by leveraging an energy source both as an energy supplier and a jammer to secure transmission under imperfections. The performance of the proposed solution is then evaluated using three key metrics (total throughput, outage probability, energy efficiency). The study highlights the significant impact of various factors such as energy harvesting, HWi, CSIi, NOMA, SICi, and FD on the performance metrics. The proposed solution also aims to prevent complete outage by optimizing required spectral efficiency, HWi, CSIi, SICi and power splitting parameter. Additionally, optimal configuration of system parameters is crucial for achieving optimum performance metrics. Furthermore, the proposed NOFE is demonstrated to be more secured than two benchmark techniques (orthogonal multiple access FD transmission and NOMA half-duplex transmission) across numerous parameter configurations, emphasizing the superiority of utilizing concurrently both NOMA and FD to only either NOMA or FD.

INDEX TERMS Nonorthogonal multiple access, channel state information imperfection, security, energy harvesting, full-duplex, hardware impairment, successive interference cancellation imperfection.

I. INTRODUCTION

A. FUNDAMENTALS

The transition from 5G to anticipated 6G systems brings with it a plethora of emerging wireless applications implemented to satisfy rigorous communication requirements for a huge quantity of devices [1], [2]. In spite of high data speed and low latency promised by these systems, their challenging issues still exist, particularly in terms of power and bandwidth allocation as the quantity of devices grows. Moreover, guaranteeing secured and reliable communication in these modern systems is a considerable interest for system designers. In response to these challenges, finding mechanisms that can concurrently meliorate energy and spectral efficiencies while guaranteeing secured and reliable transmission becomes critically important.

Nonorthogonal multiple access (NOMA) is recognized as a viable mechanism for meliorating spectral efficiency in wireless networks [3], [4]. By allocating different amounts of power to various NOMA terminals and enabling successive interference cancellation (SIC), NOMA optimizes the utilization of the available spectrum. While SIC enhances system performance, it's important to consider SIC imperfection (SICi) to ensure the reliability and effectiveness of NOMA-based systems in real-world scenarios. Also, NOMA terminals are able to scavenge wireless energy from other

The associate editor coordinating the review of this manuscript and approving it for publication was Yunlong Cai.

surrounding wireless terminals, yielding an enhanced energy efficiency. This aligns with the growing popularity and feasibility of energy harvesting (EH) circuits in the context of evolving 5G and 6G technologies [5], [6]. In addition, full-duplex (FD) communication significantly enhances spectral efficiency by enabling concurrent reception and transmission of data on the same system resource (e.g., frequency, time) [7]. This contrasts with existing half-duplex (HD) transmission, wherein reception and transmission take place separately. Accordingly, the integration of NOMA with technologies such as FD communication and EH, forming NOMA FD transmission with EH (NOFE), presents exciting opportunities for advancing the reliability, capacity, and efficiency of modern communication networks.

Channel state information (CSI) is a key knowledge source in modern communication networks, providing insight into the characteristics of the communication channel between transceivers. Despite efforts to accurately estimate CSI, limitations and imperfections can arise due to various factors such as noise, interference, mobility, and hardware constraints. These imperfections lead to CSI imperfection (CSIi), which can significantly impact the performance of wireless systems.

Hardware impairment (HWi) is an essential consideration in the design and operation of wireless communication networks. Imperfections in transceiver hardware components, such as amplifier nonlinearities, phase noise, and in-quadrature-phase imbalances, can significantly degrade system performance [8], [9], [10], [11]. Thence, HWi needs careful evaluation and analysis in system design process ere implementation.

Absolutely, promised advantages such as high energy and spectral efficiencies, as well as improved communication reliability and security can be attained by NOFE. Nevertheless, its performance is susceptible to practical imperfections like CSIi, HWi, and SICi. Accordingly, the evaluation of NOFE's performance in the presence of these imperfections is crucial for assessing its practical feasibility and effectiveness.

B. LITERATURE REVIEW

The system model in [12] considered direct NOMA (D-NOMA) from a secondary transmitter (STx) to a secondary receiver (SRx) and a primary receiver (PRx). STx is a FD user, which harvests energy and receives signals from a primary transmitter (PTx) at the same time that it conducts NOMA transmission. Transmit and receive beamformers were jointly optimized in [12]. However, [12] did not conduct the performance analysis. Reference [13] extended the work in [12] by considering the direct channel between PTx and PRx for reliability enhancement. Also, [13] conducted the performance analysis under practical imperfection (HWi). The performance analysis of cooperative NOMA (C-NOMA) was conducted in [14] under consideration of SICi. In [14], a FD relay plays two roles concurrently. It harvests energy and conducts relaying to maintain a connection between a NOMA transmitter to a far NOMA user. Nonetheless, [14] did not evaluate system performance under realistic imperfections (CSIi, HWi). References [11] and [15] analyzed the performance of relaying NOMA (R-NOMA) where a HD relay helps a NOMA transmitter in relaying its information to two NOMA receivers. The performance analysis in [11] is applicable for long-packet communication under HWi and CSIi whereas that in [15] is valid for short-packet communication. In [16], [17], and [18], a basic system model of NOFE was studied where a transmitter broadcasts a NOMA signal to a near NOMA user which is a FD device to relay information to a far NOMA user. The direct channel from the transmitter to the far user is not accounted in [16] and [18] whereas it is considered in [17]. Notwithstanding, the performance analysis was conducted under idealistic conditions without CSIi, HWi, SICi in [16], [17], and [18]. Moreover, security solutions were not a focus of [11], [12], [13], [14], [15], [16], [17], and [18].

In [19], an EH-enabled HD jammer was proposed to secure NOMA uplink transmission. Security/reliability analyses and rate optimization were conducted without accounting for practical imperfections (HWi, CSIi, SICi) in [19]. In [20], multiple near NOMA users bridge between a NOMA transmitter and a far NOMA user for reliable reception of the far NOMA user under overhearing of a wire-tapper. For complexity reduction, [20] proposed the selection of only one near NOMA user. However, near NOMA users are the HD devices and the performance analysis in [20] did not account for practical impairments (HWi, CSIi, SICi). Moreover, [20] did not propose any security solution against overhearing. The secrecy performance of R-NOMA was analyzed in [21] where a relay selection was proposed to secure the NOMA transmission from a transmitter to multiple receivers. However, only EH-enabled HD relays were considered in [21]. Reference [22] studied a system model in which an energy transmitter (ET) supplies energy to a message transmitter (MT) but also jams the wire-tapper for higher security. The system model in [22] is applicable to downlink communication. Exploiting the same idea as [22], the authors in [23] utilized ET to supply energy to legitimate unmanned aerial vehicles (UAVs) while jam illegitimate UAVs. The system model in [23] is applicable to uplink communication where legitimate UAVs transmit their messages in the NOMA manner to a base-station (BS). However, MT in [22] and legitimate UAVs in [23] worked in the HD mode. Moreover, the performance analysis ignored realistic imperfections (HWi, CSIi, SICi) in [21], [22], and [23]. The performance analysis and throughput optimization for multi-hop NOMA communication were presented in [24] where multiple EH-enabled HD UAVs serve as relays. Although the performance analysis in [24] accounted for CSIi, other practical imperfections (SICi, HWi) were not considered. Reference [25] analyzed the security/reliability performance of a basic system model of D-NOMA where one NOMA transmitter communicates with two NOMA receivers under overhearing of a wire-tapper. In [25], the wire-tapper is either active or passive. However, [25] studied only the HD

operation and its analysis neglected practical imperfections (SICi, HWi, CSIi). Furthermore, [24] and [25] did not propose any solution to secure legitimate communication. The performance of R-NOMA, where an EH-enabled HD UAV is utilized as a relay, accounting for CSIi and SICi was analyzed in [26]. The NOMA transmission is secured by artificial noise transmitted by the UAV. Nevertheless, [26] ignored HWi in its analysis. In [27], D-NOMA from MT to a close user (CU) and a distant user (DU) was secured by a FD jammer, who scavenges energy from MT. Reference [27] also analyzed key performance metrics (reliability/security system throughput (RST/SST), security/reliability energy efficiency (SEE/REE), security/reliability outage probability (SOP/ROP)) for its system model under consideration of only CSIi, ignoring other practical imperfections (HWi, SICi). Nonetheless, since the FD jammer utilizes the scavenged energy, which is usually limited, to interrupt a wire-tapping user (WU), the security capability is not improved significantly in [27].

C. CONTRIBUTIONS

The research contributes the following:

- The research introduces a novel system, NOFE. This system integrates NOMA, FD transmission, and EH to enhance energy and spectral efficiencies in wireless communication systems. Additionally, the research conducts a comprehensive performance analysis of NOFE considering practical imperfections such as SICi, CSIi, and HWi. The performance analysis of NOFE in terms of RST/SST, REE/SEE, and ROP/SOP aims to evaluate system performance in realistic scenarios.
- The research's evaluation and optimization of NOFE's performance across numerous practical scenarios provide valuable insights into the system's capability and behavior. The findings underscore the significant influences of various factors such as EH, HWi, CSIi, NOMA, FD, and SICi on NOFE's performance. Remarkably, NOFE demonstrates effectiveness in preventing complete outages by strategically adopting target spectral efficiency, HWi mitigation techniques, SICi handling methods, CSIi compensation strategies, and power splitting parameter. Moreover, optimum performance of NOFE is attained through careful configuration and optimization of system parameters. Furthermore, the proposed NOFE exhibits improved security compared to its benchmarks, orthogonal multiple access (OMA) FD transmission and NOMA HD transmission.

D. PAPER STRUCTURE

Section II describes the proposed NOFE. Subsequently, its performance metrics (RST, SST, REE, SEE, ROP, SOP) are analyzed in Section III. After that, Section IV conducts the performance analysis for two references, OMA FD transmission with EH (OFE) and NOMA HD transmission with EH (NOHE), under same conditions as NOFE to assess simultaneous influences of both FD and NOMA. Afterwards, simulation/analytical results in different practical contexts are provided in Section V for performance evaluation and comparison. Finally, Section VI closes the research.

TABLE 1. Frequently-used notations.

Notation	Meaning
$\Xi\{\cdot\}$	Expectation operator
χ_{za}	Additive noise
k_{za}	$z \to a$ channel gain
ψ	Power splitting parameter
$\mathsf{CN}(0,u)$	Zero-mean u-variance complex Gaussian random variable
φ	Fading power at 1 meter separation
λ	Efficiency of energy harvester
ϑ_{mm}	Self-interference power
ϑ_{za}	Fading power
P_e	Transmit power of WU
$\mathbb{P}\{\cdot\}$	Probability operator
P_m	Transmit power of MT
ς_{za}	CSIi
t_z	Transmit signal
ε_{za}	HWi
ν	Noise variance
$\varkappa$	Path loss exponent
$f_B(\cdot)$	Probability Density Function (PDF) of B
α_{za}	CSIi level
β_{za}	Total HWi
$F_B(\cdot)$	Cumulative Distribution Functon (CDF) of B
ι_a	SICi level
r_{za}	Received signal
$\mathsf{K}_1(\cdot)$	First-order modified Bessel function of the second kind
C	Specified spectral efficiency

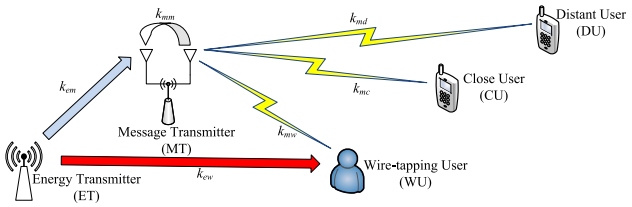

FIGURE 1. NOMA FD transmission with EH.

II. NOMA FD TRANSMISSION WITH EH

The system model demonstrated in Figure 1 exposes a specific scenario of NOFE.[1] It encompasses ET, MT, WU, CU and DU. The proposed system model can be applicable to downlink communication in wireless systems. MT is supposed to be power-constrained, hence harvesting energy from ET. ET may be a devoted energy transmitter, examples comprise a radio/television broadcasting station. MT is also a FD user, thence scavenging energy from ET and simultaneously engaging in NOMA-assisted transmission to CU and DU. Particularly, MT broadcasts a combined signal as $t = \sqrt{\psi P_m} t_d + \sqrt{(1-\psi) P_m} t_c$ wherein ψ is the

[1]The research selects NOMA for each cluster of two users, a selection inspired by prior research and existing standards. Previous research has indicated that increasing the quantity of users in each NOMA cluster can be intricate and less efficient [28], [29]. Moreover, 3GPP-LTE-A standards already incorporate two-user NOMA [30], [31]. While the research acknowledges the importance of NOMA clustering, it doesn't elaborate how to cluster a pair of users. Instead, it directs interested researchers to consult other references for a more complete understanding of NOMA clustering [3], [32], [33], [34].

power fraction allotted for transmitting t_d, P_m is the power scavenged at MT, and t_c and t_d are individual messages intended to CU and DU, respectively; $\Xi\left\{|t_l|^2\right\} = 1$, $l = \{c, d\}$. As per the NOMA mechanism, t_c is transmitted with less power than t_d. Accordingly, the parameter ψ is controlled to exceed 0.5. Additionally, MT's FD operation meliorates spectral efficiency[2] in comparison with time switching method, where communication and EH stages are separate, as well as improves EH efficiency[3] in comparison with power splitting method, where received power is divided for EH and communication [14]. On account of the broadcast characteristic of wireless propagation, MT's communication is eavesdropped by WU. To secure MT's communication, ET also acts as a jammer, intentionally interfering with the reception of WU. This enhances the security of MT's communication by disrupting eavesdropping attempts.

Figure 1 depicts k_{za}, $za = \{em, ew, mc, md, mw\}$, as channel gain. The research supposes independent slow flat links to suffer Rayleigh fading. Thence, the CDF and PDF of the power gain $|k_{za}|^2$ are correspondingly represented as

$$F_{|k_{za}|^2}(u) = 1 - e^{-\frac{u}{\vartheta_{za}}}, \tag{1}$$

$$f_{|k_{za}|^2}(u) = \frac{1}{\vartheta_{za}} e^{-\frac{u}{\vartheta_{za}}}, \tag{2}$$

wherein the fading power is denoted as $\vartheta_{za} = \Xi\left\{|k_{za}|^2\right\}$. The research models ϑ_{za} as $\varphi d_{za}^{-\varkappa}$ to account for path loss. Here, $\varkappa$ is the path loss decay, φ is the fading power at 1 meter distance, and d_{za} is the transceiver separation [35]. Additionally, MT experiences self-interference (SI) from transmission to reception because of being a FD user. In Figure 1, SI is represented by the loop link with the link gain k_{mm}. It is Rayleigh-distributed, i.e., $k_{mm} \sim \mathsf{CN}(0, \vartheta_{mm})$ or the PDF of $|k_{mm}|^2$ is $f_{|k_{mm}|^2}(u) = e^{-u/\vartheta_{mm}}/\vartheta_{mm}$ [36].

Owing to the FD operation, MT receives not only the signal from ET but also SI from its transmission. Consequently, the received signal at MT is described as

$$r_m = k_{em}\sqrt{P_e}t_e + k_{mm}\sqrt{P_m}t + \chi_m, \tag{3}$$

wherein P_e is the transmit power of ET, t_e is unity-power symbol broadcasted by ET (i.e., $\Xi\left\{|t_e|^2\right\} = 1$), and $\chi_m \sim \mathsf{CN}(0, \nu)$ is additive noise at MT. Since noise power is drastically smaller than signal power, MT harvests power approximated as $P_m \approx \lambda\left(|k_{em}|^2 P_e + |k_{mm}|^2 P_m\right)$ or equivalently

$$P_m \approx \frac{\lambda|k_{em}|^2}{1 - \lambda|k_{mm}|^2} P_e, \tag{4}$$

wherein $\lambda \in (0, 1)$ represents energy converting efficiency and $|k_{mm}|^2 < \frac{1}{\lambda}$.

MT sends the NOMA signal t with the scavenged power P_m. Accounting for HWi [11] and CSIi [37], the received signal at LU = {CU, DU} is expressed as

$$\begin{aligned} r_{ml} &= (k_{ml} + \varsigma_{ml})(t + \varepsilon_{ml}) + \chi_{ml} \\ &= k_{ml}\sqrt{\psi P_m}t_d + k_{ml}\sqrt{(1-\psi)P_m}t_c \\ &\quad + \varsigma_{ml}t + (k_{ml} + \varsigma_{ml})\varepsilon_{ml} + \chi_{ml}, \end{aligned} \tag{5}$$

wherein $\chi_{ml} \sim \mathsf{CN}(0, \nu)$ is additive noise at LU, $\varsigma_{ml} \sim \mathsf{CN}(0, \alpha_{ml})$ is CSIi of the MT→LU link, and $\varepsilon_{ml} \sim \mathsf{CN}(0, \beta_{ml}P_m)$ is HWi at MT and LU wherein β_{ml} is the aggregate HWi at MT and LU. As per [37], α_{ml} is represented to be $\alpha_{ml} = \gamma_{ml}\vartheta_{ml}$ wherein $\gamma_{ml} \in [0, 1)$ represents the degree of CSIi of the MT→LU link.

The decoding process at LU involves restoring its individual message t_l relied upon the received signal r_{ml}, which is given in (5). Particularly, DU employs a NOMA-based decoding process to restore its individual message t_d directly from r_{md} without decoding t_c. This is owing to power distribution ($\psi > 0.5$), which ensures that t_d is allocated more power than t_c. Accordingly, SINR[4] for DU to restore t_d is calculated from $r_{md} = k_{md}\sqrt{\psi P_m}t_d + k_{md}\sqrt{(1-\psi)P_m}t_c + \varsigma_{md}t + (k_{md} + \varsigma_{md})\varepsilon_{md} + \chi_{md}$ as

$$\Upsilon_d^{t_d} = \frac{\psi P_m|k_{md}|^2}{(1 - \psi + \beta_{md})P_m|k_{md}|^2 + (1 + \beta_{md})\alpha_{md}P_m + \nu}. \tag{6}$$

Also owing to power distribution ($\psi > 0.5$), CU first recovers DU's message t_d whilst considering t_c as interference and subsequently deletes interference induced by t_d before restoring CU's individual message t_c. Then, CU recovers t_d with SINR, calculated from $r_{mc} = k_{mc}\sqrt{\psi P_m}t_d + k_{mc}\sqrt{(1-\psi)P_m}t_c + \varsigma_{mc}t + (k_{mc} + \varsigma_{mc})\varepsilon_{mc} + \chi_{mc}$, as

$$\Upsilon_c^{t_d} = \frac{\psi P_m|k_{mc}|^2}{(1 - \psi + \beta_{mc})P_m|k_{mc}|^2 + (1 + \beta_{mc})\alpha_{mc}P_m + \nu}. \tag{7}$$

After removing the interference injected by t_d, CU performs decoding t_c. Owing to SICi, the residual interference is available after removing t_d. Let ι_c, $0 \le \iota_c \le 1$, represent the SICi level where $\iota_c = 0$ stands for completely perfect SIC while $\iota_c = 1$ implies completely imperfect SIC. Then, CU decodes t_c with SNR,[5] calculated from $\tilde{r}_{mc} = k_{mc}\sqrt{(1-\psi)P_m}t_c + \iota_c k_{mc}\sqrt{\psi P_m}t_d + \varsigma_{mc}t + (k_{mc} + \varsigma_{mc})\varepsilon_{mc} + \chi_{mc}$, as

$$\Upsilon_c^{t_c} = \frac{(1 - \psi)P_m|k_{mc}|^2}{\left(\iota_c^2\psi + \beta_{mc}\right)P_m|k_{mc}|^2 + (1 + \beta_{mc})\alpha_{mc}P_m + \nu}. \tag{8}$$

[2] In FD communication, MT performs both transmit and receive operations simultaneously within the same stage.

[3] In the context of FD transmission, MT adopts a specific strategy for EH and communication. Unlike traditional HD transmission where the received signal is split into separate paths for communication and EH, in FD transmission, MT does not split the received signal. Alternatively, MT scavenges energy from the entire received signal while simultaneously performing communication. Moreover, FD transmission inherently involves self-interference, where the transmit signal is reflected back into the receiver. In NOFE, this self-interference is leveraged for energy harvesting. By recycling the self-interference, MT can harvest a higher amount of energy, thereby improving energy efficiency and reducing reliance on external energy sources.

[4] SINR means signal-to-interference plus noise ratio.

[5] SNR represents signal-to-noise ratio.

In the meantime, WU overhears the NOMA signal t transmitted by MT but suffers the interference induced by ET. Therefore, by accounting for HWi [11] and CSIi [37], the signal received at WU is expressed as

$$\begin{aligned} r_w &= (k_{ew}+\varsigma_{ew})\left(\sqrt{P_e}t_e+\varepsilon_{ew}\right) \\ &\quad +(k_{mw}+\varsigma_{mw})\,(t+\varepsilon_{mw})+\chi_{mw} \\ &= k_{mw}\sqrt{\psi P_m}t_d+k_{mw}\sqrt{(1-\psi)\,P_m}t_c+\varsigma_{mw}t \\ &\quad +(k_{mw}+\varsigma_{mw})\,\varepsilon_{mw}+\chi_{mw}+(k_{ew}+\varsigma_{ew})\left(\sqrt{P_e}t_e+\varepsilon_{ew}\right), \end{aligned} \tag{9}$$

wherein $\chi_{mw} \sim \mathsf{CN}(0,\nu)$ is additive noise at WU, AT $=$ {ET, MT}, $\varsigma_{aw} \sim \mathsf{CN}(0,\alpha_{aw})$ is CSIi of the AT$\rightarrow$WU link, $a = \{e,m\}$, and $\varepsilon_{aw} \sim \mathsf{CN}(0,\beta_{aw}P_a)$ is HWi at AT and WU wherein β_{aw} is the aggregate HWi at AT and WU. As per [37], α_{aw} is represented to be $\gamma_{aw}\vartheta_{aw}$ wherein $\gamma_{aw} \in [0,1)$ represents the degree of CSIi of the AT$\rightarrow$WU link.

According to (9), WU conducts decoding of t_c and t_d using the NOMA-based decoding process. Owing to power distribution ($\psi > 0.5$), WU first restores DU's message t_d, treating t_c as interference. Afterward, WU deletes the interference injected by t_d before decoding t_c. Then, SINR for WU to recover t_d is inferred from (9) as (10), shown at the bottom of the next page.

After suppressing the interference generated by t_d, WU performs its decoding process to recover CU's message t_c. However, owing to SICi, there may still be residual interference present after suppressing t_d. Let ι_w, $0 \le \iota_w \le 1$, represent the SICi level where $\iota_w = 0$ stands for completely perfect SIC while $\iota_w = 1$ implies completely imperfect SIC. Then, WU recovers t_c with SNR, calculated from $\tilde{r}_w = \iota_w k_{mw}\sqrt{\psi P_m}t_d + k_{mw}\sqrt{(1-\psi)\,P_m}t_c + \varsigma_{mw}t + (k_{mw}+\varsigma_{mw})\,\varepsilon_{mw}+\chi_{mw}+(k_{ew}+\varsigma_{ew})\left(\sqrt{P_e}t_e+\varepsilon_{ew}\right)$, as (11), shown at the bottom of the next page.

One sees from (10)-(11) that ET introduces interference to WU through jamming, CSIi, and HWi. This interference is quantified as $|k_{ew}|^2\,(1+\beta_{ew})\,P_e + \alpha_{ew}\,(1+\beta_{ew})\,P_e$, which contributes drastically to degrading the probability of successful recovery of t_d and t_c at WU, thereby enhancing message security.

III. ANALYTICAL RESULTS OF NOFE

The section systematically approaches the secrecy and reliability performance analysis of NOFE, beginning with the analysis of SOP/ROP. SOP and ROP metrics indicate the likelihood that the accomplished channel capacity at the wire-tapping receiver (SOP) or the legitimate receiver (ROP) falls below the specified spectral efficiency (C). A smaller ROP implies higher reliability, indicating that the legitimate receiver is less likely to experience an outage. Conversely, a smaller SOP implies lower security, indicating that the wire-tapping receiver is more likely to successfully eavesdrop on communication. Following the SOP/ROP analysis, the section extends the evaluation to include RST, SST, REE, and SEE. These metrics provide insights into the overall system performance in terms of security and reliability, considering both throughput and energy efficiency aspects. Utilizing understandings attained from the SOP/ROP analysis, these additional analyses offer a complete assessment of the secrecy and reliability performance of NOFE. The importance of these analyses falls in their efficiency, as they offer a prompt assessment of the secrecy and reliability performance without the need for exhaustive simulations. This allows for a systematic evaluation of NOFE under various scenarios and parameter configurations, enabling system designers to make informed decisions to optimize the system's security and reliability while ensuring efficient resource utilization.

A. ROP OF DU (Θ_D^D)

Given C, Θ_d^d measures the likelihood that DU fails to recover its individual message t_d. This implies that channel capacity accomplished at DU for recovering t_d is less than C:

$$\Theta_d^d = \mathbb{P}\left\{\log_2\left(1+\Upsilon_d^{t_d}\right) < C\right\} = \mathbb{P}\left\{\Upsilon_d^{t_d} < K\right\}, \tag{12}$$

where $K = 2^C - 1$.

Inserting (6) into (12) and after some simplifications, one gets

$$\Theta_d^d = \begin{cases} \bar{\Theta}_d^d & , K < K_{dd} \\ 1 & , K \ge K_{dd} \end{cases} \tag{13}$$

where $K_{dd} = \frac{\psi}{1-\psi+\beta_{md}}$ and

$$\bar{\Theta}_d^d = \mathbb{P}\left\{|k_{md}|^2 < \frac{A_{dd}P_m + B_{dd}}{P_m}\right\}, \tag{14}$$

with $A_{dd} = \frac{K(1+\beta_{md})\alpha_{md}}{\psi - K(1-\psi+\beta_{md})}$ and $B_{dd} = \frac{\nu K}{\psi - K(1-\psi+\beta_{md})}$.

Remark 1: Given that $K_{dd} = \frac{\psi}{1-\psi+\beta_{md}}$ and $K = 2^C - 1$, (13) illustrates that DU experiences different outage levels depending on the configuration of the specified spectral efficiency (C), the HWi parameter (β_{md}), and the power splitting parameter (ψ). In particular, if C, β_{md}, and ψ are configured unreasonably such that $K_{dd} \le K$, DU suffers complete outage, i.e., $\Theta_d^d = 1$. However, complete outage of DU can be prevented by appropriately configuring C, β_{md}, and ψ such that $K_{dd} > K$. Alternatively, NOFE must restrain the target spectral efficiency such that $C < \log_2\left(\frac{1+\beta_{md}}{1-\psi+\beta_{md}}\right)$ in order for eliminating complete outage for DU. This constraint ensures that the achievable rate for DU remains below the maximum allowable rate determined by system parameters, thus preventing complete outage and ensuring reliable communication for DU.

B. ROP OF CU (Θ_C^C)

Given C, Θ_c^c measures the probability which CU fails to recover t_c. This implies the channel capacity attained at CU for recovering t_c is smaller than C:

$$\Theta_c^c = \mathbb{P}\left\{\log_2\left(1+\Upsilon_c^{t_c}\right) < C\right\} = \mathbb{P}\left\{\Upsilon_c^{t_c} < K\right\}. \tag{15}$$

Plugging (8) into (15) and conducting some simplification, one gets

$$\Theta_c^c = \begin{cases} \bar{\Theta}_c^c & , K < K_{cc} \\ 1 & , K \geq K_{cc} \end{cases} \tag{16}$$

where $K_{cc} = \frac{1-\psi}{\iota_c^2\psi+\beta_{mc}}$ and

$$\bar{\Theta}_c^c = \mathbb{P}\left\{|k_{mc}|^2 < \frac{A_{cc}P_m + B_{cc}}{P_m}\right\}, \tag{17}$$

with $A_{cc} = \frac{(1+\beta_{mc})\alpha_{mc}K}{1-\psi-(\iota_c^2\psi+\beta_{mc})K}$ and $B_{cc} = \frac{\nu K}{1-\psi-(\iota_c^2\psi+\beta_{mc})K}$.

Remark 2: Given that $K_{cc} = \frac{1-\psi}{\iota_c^2\psi+\beta_{mc}}$ and $K = 2^C - 1$, (16) illustrates that CU experiences different outage levels depending on the configuration of the target spectral efficiency (C), the HWi parameter (β_{mc}), the SICi parameter ι_c, and the power splitting parameter (ψ). In particular, if C, β_{mc}, ι_c, and ψ are configured unreasonably such that $K_{cc} \leq K$, CU suffers complete outage, i.e., $\Theta_c^c = 1$. However, complete outage of CU can be prevented by properly configuring C, β_{mc}, ι_c, and ψ such that $K_{cc} > K$. Alternatively, NOFE must restrain the target spectral efficiency such that $C < \log_2\left(1 + \frac{1-\psi}{\iota_c^2\psi+\beta_{mc}}\right)$ in order for eliminating complete outage for CU. This constraint ensures that the achievable rate for CU remains below the maximum allowable rate determined by system parameters, thus preventing complete outage and ensuring reliable communication for CU.

Remark 3: Integrating two remarks (1 and 2), it is inferred that NOFE must restrain $K < K_{cc}$ and $K < K_{dd}$, or $K < \min(K_{cc}, K_{dd})$, i.e. restrain its target spectral efficiency

$$C < \log_2\left(1 + \min\left(\frac{1-\psi}{\iota_c^2\psi+\beta_{mc}}, \frac{\psi}{1-\psi+\beta_{md}}\right)\right), \tag{18}$$

in order for eliminating complete outage for both CU and DU. Conversely, if NOFE restrains $K \geq K_{cc}$ and $K \geq K_{dd}$, or $K \geq \max(K_{cc}, K_{dd})$, both CU and DU experience complete outage. Alternatively, if NOFE configures

$$C \geq \log_2\left(1 + \max\left(\frac{1-\psi}{\iota_c^2\psi+\beta_{mc}}, \frac{\psi}{1-\psi+\beta_{md}}\right)\right), \tag{19}$$

then both CU and DU suffer complete outage.

Remark 4: (13) and (16) indeed demonstrate that the performance of both CU and DU in NOFE is impacted by numerous system parameters, including (C, ϑ_{za}, ϑ_{mm}, λ, ψ, P_e, ν, γ_{za}, β_{za}, ι_l). Accordingly, the adjustment of these parameters enables NOFE to attain specific performance targets.

Remark 5: Both $\bar{\Theta}_d^d$ in (14) and $\bar{\Theta}_c^c$ in (17) are consistently rewritten in closed-form (the proof is deferred to Appendix A) as

$$\bar{\Theta}_l^l = \frac{\pi^2}{4G}\sum_{i=1}^{G}\frac{\sqrt{1-\delta_i^2}}{\cos^2\eta_i}F_{|k_{ml}|^2}\left(\frac{A_{ll}\tan\eta_i + B_{ll}}{\tan\eta_i}\right)f_{P_m}(\tan\eta_i), \tag{20}$$

where $\delta_i = \cos\left(\frac{2i-1}{2G}\pi\right)$, $\eta_i = \frac{\pi}{4}(\delta_i + 1)$, G represents the complexity-precision trade-off, and

$$f_{P_m}(z) = H\left[\frac{M}{(z-H)^2} - \frac{e^{-Lz}}{(z-H)^2} - L\frac{e^{-Lz}}{z-H}\right], \tag{21}$$

with $H = \frac{\vartheta_{em}P_e}{\vartheta_{mm}}$, $L = \frac{1}{\vartheta_{em}P_e\lambda}$, and $M = e^{-\frac{1}{\vartheta_{mm}\lambda}}$.

By inserting (20) into (13) and (16), one obtains the closed-form representations of Θ_d^d and Θ_c^c.

C. SOP AT WU

1) SOP FOR T_D

Conditioned on C, Θ_w^d measures the likelihood that WU fails to restore DU's message (t_d). This implies the channel capacity attainable at WU for decoding t_d is less than C:

$$\Theta_w^d = \mathbb{P}\left\{\log_2\left(1 + \Upsilon_w^{t_d}\right) < C\right\} = \mathbb{P}\left\{\Upsilon_w^{t_d} < K\right\}. \tag{22}$$

Inserting (10) into (22) and conducting some manipulations, one gets

$$\Theta_w^d = \begin{cases} \bar{\Theta}_w^d & , K < K_{wm} \\ 1 & , K \geq K_{wm} \end{cases} \tag{23}$$

where $K_{wm} = \frac{\psi}{1-\psi+\beta_{mw}}$ and

$$\bar{\Theta}_w^d = \mathbb{P}\left\{|k_{mw}|^2 < A_{wd} + B_{wd}\frac{|k_{ew}|^2}{P_m} + \frac{D_{wd}}{P_m}\right\}, \tag{24}$$

with $A_{wd} = \frac{K(1+\beta_{mw})\alpha_{mw}}{\psi-K(1-\psi+\beta_{mw})}$, $B_{wd} = \frac{(1+\beta_{ew})P_eK}{\psi-K(1-\psi+\beta_{mw})}$ and $D_{wd} = \frac{[\alpha_{ew}(1+\beta_{ew})P_e+\nu]K}{\psi-K(1-\psi+\beta_{mw})}$.

Remark 6: Given that $K_{wm} = \frac{\psi}{1-\psi+\beta_{mw}}$ and $K = 2^C - 1$, (23) illustrates that WU experiences different secrecy outage levels when wire-tapping DU's message, depending on the configuration of the target spectral efficiency (C), the HWi parameter (β_{mw}), and the power splitting parameter (ψ). Specifically, WU experiences complete secrecy outage (indicating that DU's message is absolutely secured) if C, β_{mw}, and ψ are configured reasonably such that $K_{wm} \leq K$.

$$\Upsilon_w^{t_d} = \frac{\psi P_m|k_{mw}|^2}{(1-\psi+\beta_{mw})P_m|k_{mw}|^2 + (1+\beta_{mw})\alpha_{mw}P_m + \nu + |k_{ew}|^2(1+\beta_{ew})P_e + \alpha_{ew}(1+\beta_{ew})P_e} \tag{10}$$

$$\Upsilon_w^{t_c} = \frac{(1-\psi)P_m|k_{mw}|^2}{(\iota_w^2\psi+\beta_{mw})P_m|k_{mw}|^2 + (1+\beta_{mw})\alpha_{mw}P_m + \nu + |k_{ew}|^2(1+\beta_{ew})P_e + \alpha_{ew}(1+\beta_{ew})P_e} \tag{11}$$

However, complete secrecy outage does not occur if C, β_{mw}, and ψ are configured unreasonably such that $K_{wm} > K$. Alternatively, NOFE must ensure a lower bound on the target spectral efficiency such that $C \geq \log_2\left(\frac{1+\beta_{mw}}{1-\psi+\beta_{mw}}\right)$ in order to attain absolute security for DU's message. This lower bound ensures that the achievable rate for WU remains above the maximum allowable rate determined by the system parameters, thus suffering complete secrecy outage and ensuring absolute security for DU's message.

2) SOP FOR T_C

Given C, Θ_w^c measures the probability that WU unsuccessfully recovers t_c. This implies the channel capacity attainable at WU for decoding t_c is less than C:

$$\Theta_w^c = \mathbb{P}\left\{\log_2\left(1+\Upsilon_w^{t_c}\right) < C\right\} = \mathbb{P}\left\{\Upsilon_w^{t_c} < K\right\}. \quad (25)$$

Inserting (11) into (25) and performing some simplifications, one gets

$$\Theta_w^c = \begin{cases} \bar{\Theta}_w^c & , K < K_{wc} \\ 1 & , K \geq K_{wc} \end{cases} \quad (26)$$

where $K_{wc} = \frac{1-\psi}{\iota_w^2\psi+\beta_{mw}}$ and

$$\bar{\Theta}_w^c = \mathbb{P}\left\{|k_{mw}|^2 < A_{wc} + B_{wc}\frac{|k_{ew}|^2}{P_m} + \frac{D_{wc}}{P_m}\right\} \quad (27)$$

with $A_{wc} = \frac{K(1+\beta_{mw})\alpha_{mw}}{1-\psi-K\left(\iota_w^2\psi+\beta_{mw}\right)}$, $B_{wc} = \frac{(1+\beta_{ew})P_eK}{1-\psi-K\left(\iota_w^2\psi+\beta_{mw}\right)}$, and $D_{wc} = \frac{[\alpha_{ew}(1+\beta_{ew})P_e+\nu]K}{1-\psi-K\left(\iota_w^2\psi+\beta_{mw}\right)}$.

Remark 7: Given that $K_{wc} = \frac{1-\psi}{\iota_w^2\psi+\beta_{mw}}$ and $K = 2^C - 1$, (26) illustrates that WU suffers different secrecy outage levels when overhearing CU's message, depending on the configuration of the target spectral efficiency (C), the HWi parameter (β_{mw}), the SICi parameter (ι_w), and the power splitting parameter (ψ). In particular, WU experiences complete secrecy outage (indicating that CU's transmission is absolutely secured) if C, β_{mw}, ι_w, and ψ are configured reasonably such that $K_{wc} \leq K$. However, complete secrecy outage of WU does not occur if C, β_{mw}, ι_w, and ψ are configured inappropriately such that $K_{wc} > K$. Alternatively, NOFE must ensure a lower bound on the target spectral efficiency such that $C \geq \log_2\left(1+\frac{1-\psi}{\iota_w^2\psi+\beta_{mw}}\right)$ in order to attain absolute security for CU's message. This lower bound ensures that the achievable rate for WU remains above the maximum allowable rate determined by the system parameters, thus suffering complete secrecy outage and ensuring absolute security for CU's message.

Remark 8: By integrating two remarks (6 and 7), it is seen that if NOFE restrains $K < \min(K_{wm}, K_{wc})$, i.e. restrain its target spectral efficiency

$$C < \log_2\left(1+\min\left(\frac{1-\psi}{\iota_w^2\psi+\beta_{mw}}, \frac{\psi}{1-\psi+\beta_{mw}}\right)\right),$$

then both CU and DU suffer a certain degree of insecurity. Conversely, if NOFE restrains $K \geq \max(K_{wm}, K_{wc})$, both CU and DU reach absolute security. Alternatively, if NOFE configures $C \geq \log_2\left(1+\max\left(\frac{1-\psi}{\iota_w^2\psi+\beta_{mw}}, \frac{\psi}{1-\psi+\beta_{mw}}\right)\right)$, then both CU and DU achieve absolute security.

Remark 9: (23) and (26) demonstrate that the secrecy performance for both CU and DU in NOFE is impacted by numerous specifications, including (C, ϑ_{za}, ϑ_{mm}, λ, ψ, P_e, ν, γ_{aw}, ι_w, β_{aw}). Accordingly, the adjustment of these specifications permits NOFE to attain specific secrecy performance target.

Remark 10: Both $\bar{\Theta}_w^d$ in (23) and $\bar{\Theta}_w^c$ in (26) are consistently written in closed-form (the proof is deferred to Appendix B) as

$$\bar{\Theta}_w^l = \frac{\pi^2}{4G}\sum_{i=1}^{G}\tilde{\Theta}_{wl}(\tan\eta_i) f_{P_m}(\tan\eta_i)\frac{\sqrt{1-\delta_i^2}}{\cos^2\eta_i}, \quad (28)$$

where

$$\tilde{\Theta}_w^l(P_m) = 1 - \left(\frac{\vartheta_{ew}B_{wl}}{\vartheta_{mw}P_m}+1\right)^{-1} e^{-\left(A_{wl}+\frac{D_{wl}}{P_m}\right)\frac{1}{\vartheta_{mw}}}. \quad (29)$$

By inserting (28) into (23) and (26), one accomplishes the closed-form representations of Θ_w^d and Θ_w^c.

D. RELIABILITY/SECRECY SYSTEM THROUGHPUT

The throughput for NOFE under delay constraint is simply derived from the outage analysis as

$$\Delta_p^l = C\left(1-\Theta_p^l\right), \quad (30)$$

where $p = \{c, d, w\}$ and Δ_p^l is the throughput of the l whose message is decoded at the p, i.e., Δ_c^c and Δ_d^d are respectively RSTs of CU and DU whilst Δ_w^c and Δ_w^d are respectively SSTs of CU and DU.

Obviously, RST/SST in NOFE, as demonstrated by (30), is jointly affected by a set of parameters (C, ϑ_{za}, ϑ_{mm}, λ, ψ, P_e, ν, ι_q, γ_{gp}, β_{gp}) since this set affects Θ_p^l where $q = \{c, w\}$. As such, accomplishing the target RST/SST requires appropriately configuring and flexibly adjusting this set of parameters within their feasible value regions.

E. RELIABILITY/SECRECY ENERGY EFFICIENCY

In the context of communication systems, REE and SEE are important metrics that quantify the efficiency of using energy resource to reach a target transmission rate. In the scenario of NOFE, REE specifically mentions the proportion of the aggregate RSTs ($\Delta_c^c + \Delta_d^d$) to the whole power consumption (P_e). Accordingly, REE is calculated as

$$\Phi_{rel} = \frac{\Delta_c^c + \Delta_d^d}{P_e}. \quad (31)$$

Similarly, SEE is calculated as

$$\Phi_{sec} = \frac{\Delta_w^c + \Delta_w^d}{P_e}. \quad (32)$$

F. PERFORMANCE LIMIT

In communication system analysis, researching the performance upper-bound, which represents the best achievable performance that users can attain under certain conditions, is essential for gaining deep insights into the upper-bound capabilities of the system. This subsection focuses on investigating the performance limit of NOFE in scenarios where the transmit power of ET reaches infinity, i.e., $P_e \to \infty$. Analyzing the performance upper-bound under high transmit power conditions allows researchers to understand the system's behavior when energy resources are abundant and the jamming power is effectively unlimited. This analysis helps in identifying the theoretical maximum performance that can be achieved by CU, DU, and WU in NOFE, offering insights into the system's ultimate capabilities and limitations. Indeed, as $P_e \to \infty$, MT accumulates infinite power, resulting in $P_m \to \infty$. In this scenario, ROP ($\Theta_l^{l\infty}$) and SOP ($\Theta_w^{l\infty}$) for NOFE can be uniquely expressed as

$$\Theta_p^{l\infty} = \begin{cases} \bar{\Theta}_p^{l\infty} & , K_{pl} > K \\ 1 & , K_{pl} \le K \end{cases} \tag{33}$$

where

$$\bar{\Theta}_p^{l\infty} = \mathbb{P}\left\{ \left|k_{mp}\right|^2 < A_{pl} \right\} = F_{|k_{mp}|^2}\left(A_{pl}\right). \tag{34}$$

From (34), it is evident that the outage probabilities (ROP/SOP) are constrained by various factors including the corresponding channel k_{mp}, the desired spectral efficiency ($K = 2^C - 1$), the CSIi γ_{mp}, the power splitting parameter ψ, the SICi ι_q, and the HWi β_{mp}. Since the performance limit is constant, the diversity order of NOFE is indeed zero.

IV. BENCHMARK MODELS: OFE AND NOHE

Comparing NOFE with two benchmark models, OFE and NOHE, provides valuable insights into the concurrent impacts of FD and NOMA in wireless communication systems. Analyzing the performance of these benchmark models allows for a quick comparison of their reliability, energy efficiency, and security aspects. By studying their performance metrics such as throughput, outage probability, and energy efficiency, researchers can understand the trade-offs and advantages of employing FD and NOMA techniques in energy harvesting-enabled communication systems.

A. OFE

In OFE, message transmission is divided into two equal stages, each occurring within a half-second duration (transmission block is normalized to one second). During each stage, the FD operation is conducted by MT. MT harvests energy from ET and utilizes this harvested energy to broadcast messages intended for CU or DU. The transmit power P_m in this case remains the same as expressed in (4). Therefore, LU receives the signal transmitted by MT as

$$\bar{r}_{ml} = \left(k_{ml} + \varsigma_{ml}\right)\left(\sqrt{P_m}t_l + \varepsilon_{ml}\right) + \chi_{ml}. \tag{35}$$

SINR to decode t_l is calculated from (35) as

$$\bar{\Upsilon}_l^{t_l} = \frac{P_m|k_{ml}|^2}{\beta_{ml}P_m|k_{ml}|^2 + \left(1+\beta_{ml}\right)\alpha_{ml}P_m + \nu}. \tag{36}$$

ROP of LU is

$$\Theta_l^{lOMA} = \mathbb{P}\left\{ \frac{1}{2}\log_2\left(1+\bar{\Upsilon}_l^{t_l}\right) < C \right\} = \mathbb{P}\left\{ \bar{\Upsilon}_l^{t_l} < \bar{K} \right\}, \tag{37}$$

wherein $\bar{K} = 2^{2C} - 1$ and the factor $\frac{1}{2}$ ere the logarithm is proportional to the duration of each stage.

Inserting (36) into (37) results in the explicit form of Θ_l^{lOMA} as

$$\Theta_l^{lOMA} = \begin{cases} \bar{\Theta}_l^{lOMA} & , \bar{K} < \bar{K}_{ll} \\ 1 & , \bar{K} \ge \bar{K}_{ll} \end{cases} \tag{38}$$

where $\bar{K}_{ll} = \frac{1}{\beta_{ml}}$ and

$$\bar{\Theta}_l^{lOMA} = \mathbb{P}\left\{ |k_{ml}|^2 < \frac{\bar{A}_{ll}P_m + \bar{B}_{ll}}{P_m} \right\}. \tag{39}$$

with $\bar{A}_{ll} = \frac{\left(1+\beta_{ml}\right)\alpha_{ml}\bar{K}}{1-\bar{K}\beta_{ml}}$ and $\bar{B}_{ll} = \frac{\nu\bar{K}}{1-\bar{K}\beta_{ml}}$.

Both (39) and (57) have the same form. As such, (39) can be obtained in the same manner as (57), yielding (40), as shown at the bottom of the next page.

Similarly, WU receives the signal as

$$\begin{aligned} \bar{r}_{wl} = {} & k_{mw}\sqrt{P_m}t_l + \varsigma_{mw}\sqrt{P_m}t_l + \left(k_{mw} + \varsigma_{mw}\right)\varepsilon_{mw} \\ & + \chi_{mw} + \left(k_{ew} + \varsigma_{ew}\right)\left(\sqrt{P_e}t_e + \varepsilon_{ew}\right). \end{aligned} \tag{41}$$

SINR to decode t_l is calculated from (41) as (42), shown at the bottom of the next page. Then, SOP of WU is

$$\Theta_w^{lOMA} = \mathbb{P}\left\{ \frac{1}{2}\log_2\left(1+\bar{\Upsilon}_w^{t_l}\right) < C \right\} = \mathbb{P}\left\{ \bar{\Upsilon}_w^{t_l} < \bar{K} \right\}. \tag{43}$$

Substituting (42) into (43) yields the explicit form of Θ_w^{lOMA} as

$$\Theta_w^{lOMA} = \begin{cases} \bar{\Theta}_w^{lOMA} & , \bar{K} < \bar{K}_{wl} \\ 1 & , \bar{K} \ge \bar{K}_{wl} \end{cases} \tag{44}$$

where $\bar{K}_{wl} = \frac{1}{\beta_{mw}}$ and

$$\bar{\Theta}_w^{lOMA} = \mathbb{P}\left\{ |k_{mw}|^2 < \bar{A}_{wl} + \bar{B}_{wl}\frac{|k_{ew}|^2}{P_m} + \frac{\bar{D}_{wl}}{P_m} \right\}, \tag{45}$$

with $\bar{A}_{wl} = \frac{\bar{K}\left(1+\beta_{mw}\right)\alpha_{mw}}{1-\beta_{mw}}$, $\bar{B}_{wl} = \frac{\left(1+\beta_{ew}\right)P_e\bar{K}}{1-\beta_{mw}}$, and $\bar{D}_{wl} = \frac{\left[\alpha_{ew}\left(1+\beta_{ew}\right)P_e+\nu\right]\bar{K}}{1-\beta_{mw}}$.

Both (45) and (62) have the same form. As such, (45) can be obtained in the same manner as (62), yielding (46), as shown at the bottom of the next page.

By invoking (38), the formulas of RST and REE for OFE are respectively given by

$$\Delta_l^{lOMA} = \frac{C}{2}\left(1 - \Theta_l^{lOMA}\right), \tag{47}$$

and

$$\Phi_{rel}^{OMA} = \frac{\Delta_c^{cOMA} + \Delta_d^{dOMA}}{P_e}. \tag{48}$$

Similarly, by invoking (44), the formulas of SST and SEE for OFE are respectively written as

$$\Delta_w^{lOMA} = \frac{C}{2}\left(1 - \Theta_w^{lOMA}\right), \tag{49}$$

and

$$\Phi_{sec}^{OMA} = \frac{\Delta_w^{cOMA} + \Delta_w^{dOMA}}{P_e}. \tag{50}$$

Obviously, comparing the performance of NOFE with OFE offers deep understandings on the advantages of NOMA over OMA, particularly in the scenario of CSIi, HWi, SICi, FD, and EH. By assessing key metrics such as outage probability, energy efficiency, and system throughput, we determine the impact of NOMA's simultaneous transmission and power allocation strategy on system performance. Such a comparison enables a complete understanding of the benefits and trade-offs in association with diverse multiple access mechanisms in the investigated wireless communication context. The prompt performance comparison between NOFE and OFE is facilitated by the explicit formulas of Θ_p^{lOMA}, Δ_p^{lOMA}, Φ_{sec}^{OMA}, and Φ_{rel}^{OMA}. These formulas allow for a quick assessment of the relative performance of the two models under various operating conditions, aiding in the selection of the most suitable approach for specific application scenarios.

B. NOHE

In NOHE,[6] message transmission is split into two equal stages, each occurring within a half-second duration (transmission block is also normalized in one second). MT performs the HD operation. During the first stage, MT harvests energy from ET. The energy harvested during this stage is $\bar{E}_m = \frac{\lambda}{2}|k_{em}|^2 P_e$. In the second stage, MT utilizes the harvested energy to conduct NOMA communication to both CU and DU. The transmit power during this stage is $\bar{P}_m = \frac{\bar{E}_m}{0.5} = \lambda|k_{em}|^2 P_e$ whose PDF is straightforwardly derived as $f_{\bar{P}_m}(z) = Je^{-Jz}$ where $J = \frac{1}{\vartheta_{em}\lambda P_e}$. Since the signal processing in the second stage of NOHE is similar to that of NOFE, the analytical results for NOHE can be summarized based on the corresponding expressions derived for NOFE.

ROP of LU is

$$\Theta_l^{lHD} = \mathbb{P}\left\{\frac{1}{2}\log_2\left(1 + \Upsilon_l^{t_l}\right) < C\right\} = \begin{cases} \bar{\Theta}_l^{lHD} & , \bar{K} < K_{ll} \\ 1 & , \bar{K} \geq K_{ll} \end{cases} \tag{51}$$

where

$$\begin{aligned} \bar{\Theta}_l^{lHD} &= \mathbb{P}\left\{|k_{ml}|^2 < \frac{\tilde{A}_{ll}\bar{P}_m + \tilde{B}_{ll}}{\bar{P}_m}\right\} \\ &= \int_0^\infty F_{|k_{ml}|^2}\left(\frac{\tilde{A}_{ll}z + \tilde{B}_{ll}}{z}\right) f_{\bar{P}_m}(z)\, dz \\ &= \int_0^\infty \left(1 - e^{-\frac{\tilde{A}_{ll}z + \tilde{B}_{ll}}{\vartheta_{ml}z}}\right) Je^{-Jz} dz \\ &\overset{(*)}{=} 1 - e^{-\frac{\tilde{A}_{ll}}{\vartheta_{ml}}} J \int_0^\infty e^{-\frac{\tilde{B}_{ll}}{\vartheta_{ml}z} - Jz} dz \\ &= 1 - 2Je^{-\frac{\tilde{A}_{ll}}{\vartheta_{ml}}} \sqrt{\frac{\tilde{B}_{ll}}{\vartheta_{ml}J}} \mathsf{K}_1\left(2\sqrt{J\frac{\tilde{B}_{ll}}{\vartheta_{ml}}}\right), \end{aligned} \tag{52}$$

where $\overset{(*)}{=}$ is computed with [39, eq. (3.471)], $\tilde{A}_{cc} = \frac{(1+\beta_{mc})\alpha_{mc}\bar{K}}{1-\psi-(\iota_c^2\psi+\beta_{mc})\bar{K}}$, $\tilde{B}_{cc} = \frac{\nu\bar{K}}{1-\psi-(\iota_c^2\psi+\beta_{mc})\bar{K}}$, $\tilde{A}_{dd} = \frac{\bar{K}(1+\beta_{md})\alpha_{md}}{\psi-\bar{K}(1-\psi+\beta_{md})}$, and $\tilde{B}_{dd} = \frac{\nu\bar{K}}{\psi-\bar{K}(1-\psi+\beta_{md})}$.

Similarly, SOP of t_l at WU is

$$\Theta_w^{lHD} = \mathbb{P}\left\{\frac{1}{2}\log_2\left(1 + \Upsilon_w^{t_l}\right) < C\right\} = \begin{cases} \bar{\Theta}_w^{lHD} & , \bar{K} < K_{wl} \\ 1 & , \bar{K} \geq K_{wl} \end{cases} \tag{53}$$

$$\bar{\Theta}_l^{lOMA} = \frac{\pi^2}{4G}\sum_{i=1}^{G} \frac{\sqrt{1-\delta_i^2}}{\cos^2\eta_i} F_{|k_{ml}|^2}\left(\frac{\bar{A}_{ll}\tan\eta_i + \bar{B}_{ll}}{\tan\eta_i}\right) f_{P_m}(\tan\eta_i) \tag{40}$$

$$\bar{\Upsilon}_w^{t_l} = \frac{P_m|k_{mw}|^2}{\beta_{mw}P_m|k_{mw}|^2 + (1+\beta_{mw})\alpha_{mw}P_m + \nu + |k_{ew}|^2(1+\beta_{ew})P_e + \alpha_{ew}(1+\beta_{ew})P_e} \tag{42}$$

$$\bar{\Theta}_w^{lOMA} = \frac{\pi^2}{4G}\sum_{i=1}^{G}\left[1 - \left(\frac{\vartheta_{ew}\bar{B}_{wl}}{\vartheta_{mw}\tan\eta_i} + 1\right)^{-1} e^{-\left(\bar{A}_{wl} + \frac{\bar{D}_{wl}}{\tan\eta_i}\right)\frac{1}{\vartheta_{mw}}}\right] f_{P_m}(\tan\eta_i)\frac{\sqrt{1-\delta_i^2}}{\cos^2\eta_i} \tag{46}$$

[6] NOHE is the system model in [22] and [23]. Nevertheless, the performance analysis did not account for practical imperfections (HWi, CSIi, SICi).

where $\tilde{A}_{wc} = \frac{\bar{K}(1+\beta_{mw})\alpha_{mw}}{1-\psi-\bar{K}(\iota_w^2\psi+\beta_{mw})}$, $\tilde{B}_{wc} = \frac{(1+\beta_{ew})P_e\bar{K}}{1-\psi-\bar{K}(\iota_w^2\psi+\beta_{mw})}$, $\tilde{D}_{wc} = \frac{[\alpha_{ew}(1+\beta_{ew})P_e+\nu]\bar{K}}{1-\psi-\bar{K}(\iota_w^2\psi+\beta_{mw})}$, $\tilde{A}_{wd} = \frac{\bar{K}(1+\beta_{mw})\alpha_{mw}}{\psi-\bar{K}(1-\psi+\beta_{mw})}$, $\tilde{B}_{wd} = \frac{(1+\beta_{ew})P_e\bar{K}}{\psi-\bar{K}(1-\psi+\beta_{mw})}$, $\tilde{D}_{wd} = \frac{[\alpha_{ew}(1+\beta_{ew})P_e+\nu]\bar{K}}{\psi-\bar{K}(1-\psi+\beta_{mw})}$, and $\bar{\Theta}_w^{lHD}$ in (54), as shown at the bottom of the next page.

By invoking (51), the formulas of RST and REE for NOHE are derived as

$$\Delta_l^{lHD} = \frac{C}{2}\left(1-\Theta_l^{lHD}\right) \text{ and } \Phi_{rel}^{HD} = \frac{\Delta_c^{cHD}+\Delta_d^{dHD}}{P_e}. \tag{55}$$

Similarly, by utilizing (53), the formulas of SST and SEE for NOHE are written as

$$\Delta_w^{lHD} = \frac{C}{2}\left(1-\Theta_w^{lHD}\right) \text{ and } \Phi_{sec}^{HD} = \frac{\Delta_w^{cHD}+\Delta_w^{dHD}}{P_e}. \tag{56}$$

Obviously, comparing the performance of NOFE with NOHE provides valuable insights into the advantages of FD over HD, particularly in the scenario of EH, NOMA, CSIi, HWi, and SICi. By assessing metrics such as system throughput, energy efficiency, and outage probability, one can observe the influence of FD on the overall system performance. Utilizing the closed-form formulas of Θ_p^{lHD}, Δ_p^{lHD}, Φ_{rel}^{HD}, and Φ_{sec}^{HD}, performance comparison between NOFE and NOHE can be efficiently and quickly conducted. This comparison aids in understanding the benefits and trade-offs associated with employing FD in the considered wireless communication scenario, providing valuable insights for system design and optimization.

V. RESULTS AND DISCUSSION

The section provides a comprehensive evaluation of the performance of NOFE in various scenarios, including pivotal parameters and comparisons with its counterparts, OFE and NOHE. Both analytical (Ana)[7] and simulation (Sim)[8] evaluations are conducted to ensure the accuracy of the results. The system parameters are defined to simulate realistic conditions, with users arbitrarily located in a two-dimensional plane. The parameters used in the simulations are as follows, unless otherwise reported: ET $(0, 10)$, MT $(0, 0)$, WU $(20, 20)$, CU $(40, 0)$, DU $(50, 5)$, the energy converting efficiency $\lambda = 0.5$, the path-loss decay $\varkappa = 2.8$, the level of the CSIi $\gamma_{za} = \gamma = 0.01$, the self-interference power $\vartheta_{mm} = -50$ dB, the total HWi $\beta_{za} = \beta = 0.1$, the specified spectral efficiency $C = 0.5$ bps/Hz, the SICi level $\iota_q^2 = \iota^2 = 0.1$, the power splitting parameter $\psi = 0.9$, the noise power $\nu = -90$ dBm, the reference fading power $\varphi = -10$ dB, and the transmit power of ET $P_e = 30$ dBm.

The gap between the aggregate reliability throughputs and the aggregate security throughputs, represented as TPg_Q, serves as a pivotal performance metric in comparing the models $\text{Q} = \{\text{NOFE, OFE, NOHE}\}$. Additionally, the energy efficiency gap, EEg_Q, which is TPg_Q normalized by the transmit power P_e, is also considered. One notes that $\text{TPg}_\text{Q} = \left(\Delta_c^c + \Delta_d^d\right) - \left(\Delta_w^c + \Delta_w^d\right)$. TPg_Q and EEg_Q behave similarly to secrecy capacity, which represents the gap between capacity at legitimate receiver and that at WU [36]. Thus, a higher TPg_Q (EEg_Q) indicates better security. The subsequent results in Figures 2-9 demonstrate the consistency between the analytical and simulation results, validating the accuracy of the derived formulas in Sections III-IV. This consistency ensures confidence in the analytical framework and provides insights into the performance of NOFE compared to OFE and NOHE under various conditions.

Figure 2 compares the security performance in terms of throughput gap for the three considered models (NOFE, OFE, NOHE) with respect to (wrt) P_e. It is evident that the performance of NOFE saturates at high P_e, consistent with the analysis in Subsection III-F. However, the saturated throughput gap of NOFE is nearly double that of OFE and more than three times that of NOHE, highlighting the superiority of the proposed model (NOFE) over its benchmark models (OFE, NOHE). In addition, the performances of all three system models improve with increasing P_e, attributed to the increase in the amount of scavenged energy. Furthermore, the proposed system model (NOFE) considerably outperforms its counterparts, demonstrating the remarkable effectiveness of using concurrently FD and NOMA compared to solely employing either FD or NOMA. Remarkably, FD provides a notably higher throughput gap than HD, as evident from the considerably higher throughput gap of NOFE and OFE compared to NOHE. This gap stems from the fact that the throughput of FD can be double that of HD.

Figure 3 compares throughput gap among the three system models wrt C. Apparently, the proposed system model is dramatically superior to its counterparts across the entire range of C, demonstrating the notable effectiveness of concurrently using FD and NOMA compared to solely employing either FD or NOMA. Remarkably, FD provides a significantly higher throughput gap than HD, as evidenced by the notably higher throughput gap of NOFE and OFE compared to NOHE. This difference arises from the fact that the throughput of FD can be double that of HD. Interestingly, when C exceeds a certain threshold (e.g., $C >$ 2.46 bps/Hz in Figure 3), both CU and DU in the proposed system model experience full outage (or zero throughput gap). The threshold 2.46 bps/Hz is already derived in (19), reaffirming the accuracy of the proposed derivations and valuable understandings they provide. Moreover, C can be optimally computed to attain the peak throughput gap for the three considered system models. This is logical since the throughput is the multiplication of C and $\left(1-\Theta_p^l\right)$ (e.g., see (30)) wherein Θ_p^l is proportional to C. For

[7]The analytical evaluations are conducted by using formulas derived in Sections III-IV.

[8]The simulation evaluations are conducted by using Monte-Carlo simulations.

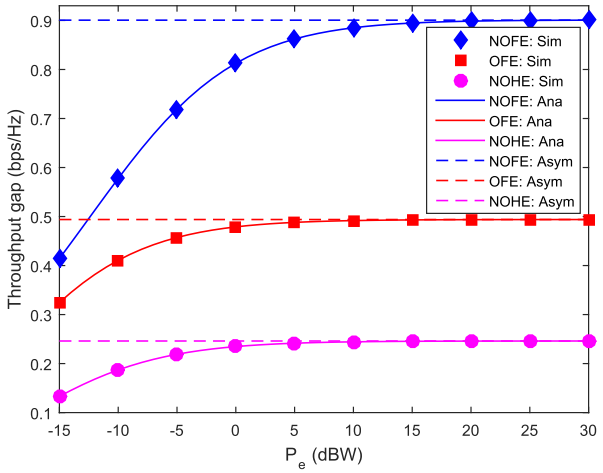

FIGURE 2. Throughput gap wrt P_e. "Asym" means Asymptote (i.e., throughput gap at high P_e).

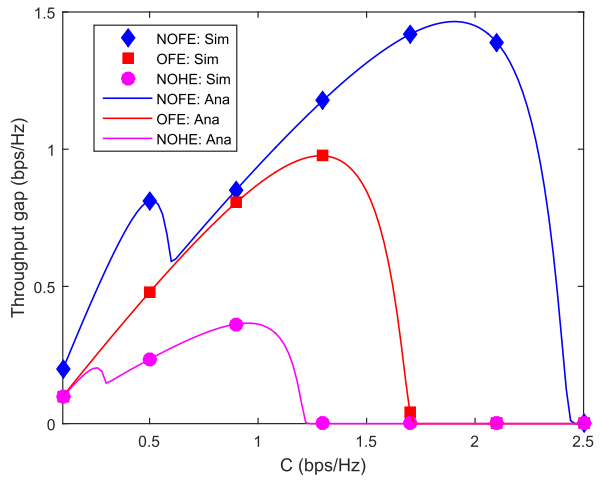

FIGURE 3. Throughput gap wrt C.

instance, NOFE, OFE, and NOHE respectively reach the peak throughput gap at $C = 1.9, 1.28, 0.96$ bps/Hz.

Figure 4 compares the secrecy performance among the three considered system models for varying γ, which represents the severity of CSIi. It is apparent that the proposed system model surpasses its counterparts across the entire range of γ, once again highlighting the notable effectiveness

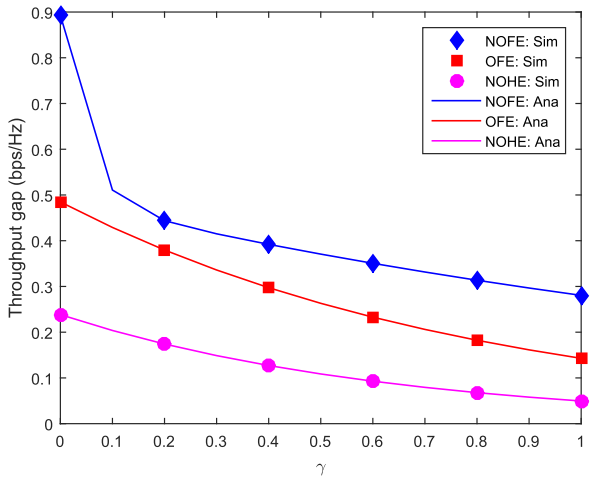

FIGURE 4. Throughput gap wrt γ.

of concurrently exploiting FD and NOMA compared to solely employing either FD or NOMA. Notably, FD provides significantly higher security than HD, as evidenced by the notably higher security achieved by NOFE and OFE compared to NOHE. This difference arises from the fact that the throughput of FD can be double that of HD. Additionally, all the investigated system models experience considerable performance degradation with increasing γ. This degradation is expected since higher values of γ indicate more severe CSIi, which adversely affects system performance.

Figure 5 compares the security performance among the three considered system models for varying β, representing the severity of HWi. Apparently, the proposed system model (NOFE) outperforms its counterparts across the entire range of β, once again highlighting the notable effectiveness of concurrently exploiting FD and NOMA compared to solely employing either FD or NOMA. Remarkably, FD provides significantly higher security than HD, as evidenced by the notably higher security achieved by NOFE and OFE compared to NOHE. This difference arises from the fact that the throughput of FD can be double that of HD. Additionally, it is observed that NOFE suffers a significant security degradation with increasing β, while its counterparts are almost unaffected by β. This indicates that NOFE's security performance is more sensitive to the severity of HWi compared to OFE and NOHE. Notably, NOFE

$$\begin{aligned}\bar{\Theta}_w^{lHD} &= \mathbb{P}\left\{|k_{mw}|^2 < \tilde{A}_{wl} + \tilde{B}_{wl}\frac{|k_{ew}|^2}{\bar{P}_m} + \frac{\tilde{D}_{wl}}{\bar{P}_m}\right\} \\ &= \int_0^\infty \tilde{\Theta}_{wl}(y) f_{\bar{P}_m}(y)\, dy \\ &= \frac{\pi^2 J}{4G}\sum_{i=1}^{G}\left[1 - \left(\frac{\vartheta_{ew}\tilde{B}_{wl}}{\vartheta_{mw}\tan\eta_i} + 1\right)^{-1} e^{-\left(\tilde{A}_{wl} + \frac{\tilde{D}_{wl}}{\tan\eta_i}\right)\frac{1}{\vartheta_{mw}}}\right] e^{-J\tan\eta_i}\frac{\sqrt{1-\delta_i^2}}{\cos^2\eta_i} \end{aligned} \tag{54}$$

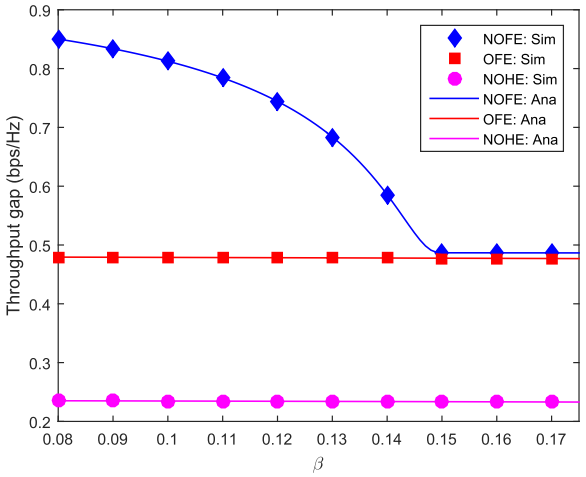

FIGURE 5. Throughput gap wrt β. Particular values of β are from 0.08 to 0.175 as per [40].

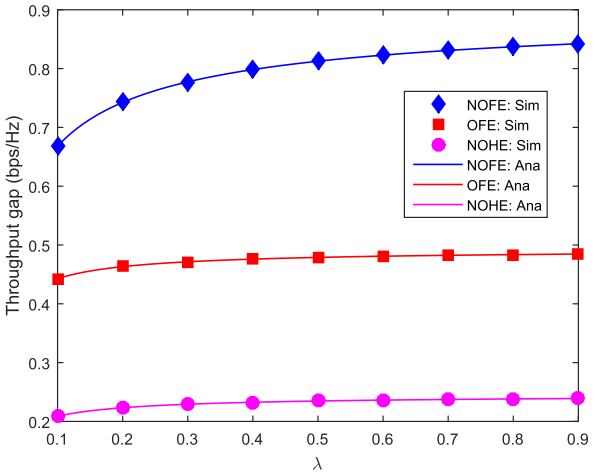

FIGURE 7. Throughput gap wrt λ.

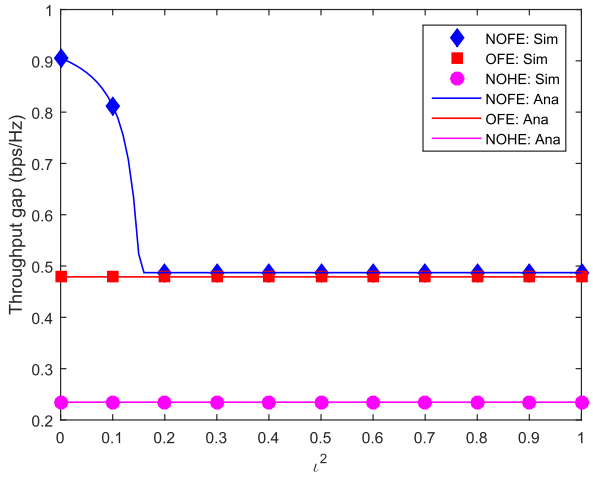

FIGURE 6. Throughput gap wrt ι^2.

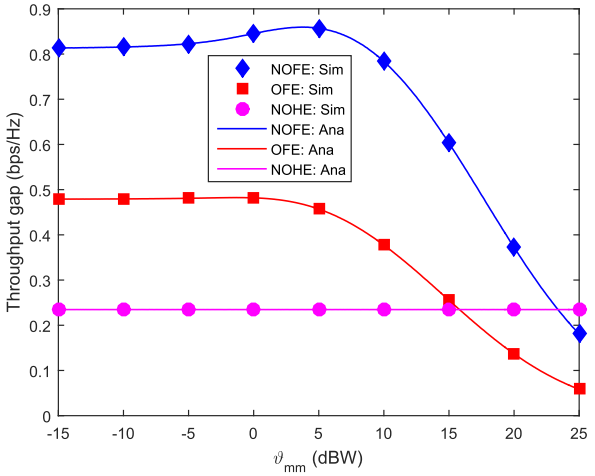

FIGURE 8. Throughput gap wrt ϑ_{mm}.

saturates at high severity of HWi, indicating a limit to its performance improvement in the presence of severe hardware impairments.

Figure 6 compares the security performance among the three considered system models for varying ι, representing the severity of SICi. Obviously, the proposed system model (NOFE) achieves higher security than its counterparts across the entire range of ι, once again highlighting the notable effectiveness of concurrently exploiting FD and NOMA compared to solely employing either FD or NOMA. Remarkably, FD provides significantly higher security than HD, as evidenced by the notably higher security achieved by NOFE and OFE compared to NOHE. This difference arises from the fact that the throughput of FD can be double that of HD. Additionally, it is observed that NOFE suffers a significant security degradation with increasing ι, while its counterparts are almost unaffected by ι. This indicates that NOFE's security performance is more sensitive to the severity of SICi compared to OFE and NOHE. Notably, NOFE quickly saturates at high severity of SICi, for instance, $\iota^2 \geq 0.15$, indicating a limit to its performance improvement in the presence of severe SICi.

Figure 7 compares the security performance of NOFE with that of OFE and NOHE wrt the efficiency of the energy harvester λ. Apparently, the proposed system model (NOFE) consistently outperforms its counterparts across the entire range of λ, once again highlighting the notable effectiveness of concurrently exploiting FD and NOMA compared to solely employing either FD or NOMA. Remarkably, FD provides significantly higher security than HD, as evidenced by the notably higher security achieved by NOFE and OFE compared to NOHE. This difference arises from the fact that the throughput of FD can be double that of HD. Additionally, increasing λ, which results in a higher amount of harvested energy, significantly enhances the security for NOFE, whereas it only slightly improves the security for OFE and NOHE, as anticipated.

Figure 8 compares the security performance of NOFE with two reference models (OFE and NOHE) wrt the

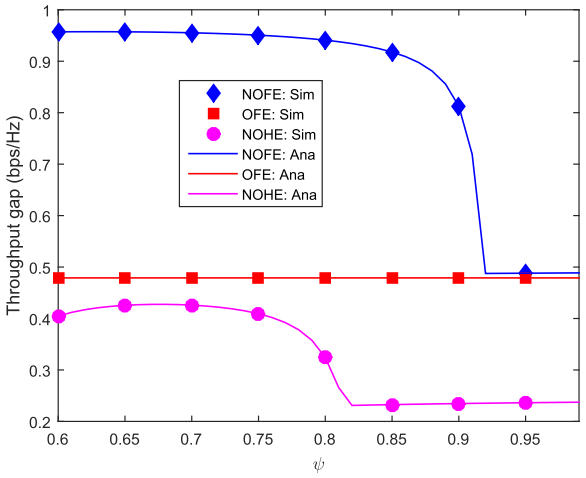

FIGURE 9. Throughput gap wrt ψ.

self-interference power ϑ_{mm}. It is evident that the proposed system model (NOFE) consistently outperforms its counterparts across the entire range of ϑ_{mm}, once again highlighting the notable effectiveness of concurrently exploiting FD and NOMA compared to solely employing either FD or NOMA. Remarkably, FD provides significantly higher security than HD, as evidenced by the notably higher security achieved by NOFE and OFE compared to NOHE. This difference arises from the fact that the throughput of FD can be double that of HD. Additionally, as expected, the performances of NOFE and OFE are influenced by ϑ_{mm}, while that of NOHE remains unchanged with changing ϑ_{mm}.

Figure 9 illustrates the comparison of security performance among NOFE and two reference models (OFE and NOHE) wrt the power splitting parameter ψ. It is evident that NOFE consistently outperforms its counterparts across the entire range of ψ, highlighting the notable effectiveness of concurrently exploiting FD and NOMA compared to solely employing either FD or NOMA. Remarkably, FD provides significantly higher security than HD, as evidenced by the notably higher security achieved by NOFE and OFE compared to NOHE. This difference arises from the fact that the throughput of FD can be double that of HD. Additionally, as expected, the performances of NOFE and NOHE are influenced by ψ, while that of OFE remains unchanged with changing ψ. Notably, all considered system models saturate at high ψ, suggesting a limit to the achievable security improvement with increasing power splitting parameter.

VI. CONCLUSION

The paper offers a thorough exploration of NOFE, particularly in the presence of realistic impairments like CSIi, HWi, and iCSI. By providing explicit formulas, it enables a swift and effective evaluation of system metrics such as throughput, energy efficiency, and outage probability across a wide range of crucial parameters. Key insights from the study include the significant impact of FD, NOMA, SI, EH, CSIi, HWi, and SICi on system performance. Notably, NOFE demonstrates the capability to mitigate full outage through careful parameter tuning and attain optimum performance under specific settings. Furthermore, the comparative analysis with reference models (OFE and NOHE) sheds light on the advantages of concurrently leveraging NOMA and FD over solely employing either NOMA or FD. This highlights the superior performance of NOFE across diverse parameter settings, providing valuable insights for future research and practical implementations.

APPENDIX A: THE PROOF OF (20)

Both $\bar{\Theta}_d^d$ in (14) and $\bar{\Theta}_c^c$ in (17) are consistently rewritten as

$$\bar{\Theta}_l^l = \mathbb{P}\left\{|k_{ml}|^2 < \frac{A_{ll}P_m + B_{ll}}{P_m}\right\}, \tag{57}$$

which is explicitly computed as

$$\bar{\Theta}_l^l = \int_0^\infty F_{|k_{ml}|^2}\left(\frac{A_{ll}z + B_{ll}}{z}\right) f_{P_m}(z)\, dz, \tag{58}$$

where $f_{P_m}(z)$ has a closed-form representation as (21), which is proved as follows.

Invoking P_m in (4), its CDF is expressed as

$$\begin{aligned} F_{P_m}(z) &= \mathbb{P}\{P_m < z\} \\ &= \mathbb{P}\left\{\frac{\lambda|k_{em}|^2}{1-\lambda|k_{mm}|^2}P_e < z\right\} \\ &= \int_0^{\frac{1}{\lambda}} F_{|k_{em}|^2}\left([1-\lambda y]\frac{z}{P_e\lambda}\right) f_{|k_{mm}|^2}(y)\, dy. \end{aligned} \tag{59}$$

By using the explicit formulas of $F_{|k_{em}|^2}(\cdot)$ and $f_{|k_{mm}|^2}(\cdot)$, the closed-form representation of $F_{P_m}(z)$ is

$$\begin{aligned} F_{P_m}(z) &= \int_0^{\frac{1}{\lambda}} \left(1 - e^{-\frac{1}{\vartheta_{em}}[1-\lambda y]\frac{z}{P_e\lambda}}\right)\frac{e^{-y/\vartheta_{mm}}}{\vartheta_{mm}} dy \\ &= F_{|k_{mm}|^2}\left(\frac{1}{\lambda}\right) + \left(\frac{\vartheta_{mm}z}{\vartheta_{em}P_e} - 1\right)^{-1}\left(e^{-\frac{z}{\vartheta_{em}P_e\lambda}} - e^{-\frac{1}{\vartheta_{mm}\lambda}}\right). \end{aligned} \tag{60}$$

The CDF of P_m, $f_{P_m}(z)$, is derived by taking the derivative of $F_{P_m}(z)$ with respect to z, yielding (21).

Now, by applying a variable change $z = \tan y$, (58) is further expressed as

$$\bar{\Theta}_l^l = \int_0^{\pi/2} F_{|k_{ml}|^2}\left(\frac{A_{ll}\tan y + B_{ll}}{\tan y}\right) f_{P_m}(\tan y)\frac{dy}{\cos^2 y}. \tag{61}$$

Utilizing Gaussian-Chebyshev quadrature in [38], (61) is strictly approximated as (20), finishing the proof.

APPENDIX B: THE PROOF OF (28)

Both $\bar{\Theta}_w^d$ in (23) and $\bar{\Theta}_w^c$ in (26) are consistently written as

$$\bar{\Theta}_w^l = \mathbb{P}\left\{|k_{mw}|^2 < A_{wl} + B_{wl}\frac{|k_{ew}|^2}{P_m} + \frac{D_{wl}}{P_m}\right\}, \tag{62}$$

which is explicitly computed as (63).

$$\bar{\Theta}_w^l = \Xi_{P_m}\left\{\underbrace{\int_0^\infty F_{|k_{mw}|^2}\left(A_{wl} + B_{wl}\frac{y}{P_m} + \frac{D_{wl}}{P_m}\right) f_{|k_{ew}|^2}(y)\,dy}_{\tilde{\Theta}_w^l(P_m)}\right\} \tag{63}$$

Utilizing the explicit formulas of $F_{|k_{mw}|^2}(\cdot)$ in (1) and $f_{|k_{ew}|^2}(\cdot)$ in (2), one reduces $\tilde{\Theta}_w^l(P_m)$ in (63) to

$$\tilde{\Theta}_w^l(P_m) = \int_0^\infty \left(1 - e^{-\left(A_{wl} + B_{wl}\frac{y}{P_m} + \frac{D_{wl}}{P_m}\right)\frac{1}{\vartheta_{mw}}}\right)\frac{1}{\vartheta_{ew}} e^{-\frac{y}{\vartheta_{ew}}}\,dy, \tag{64}$$

which is straightforwardly derived in the closed-form representation as (29).

Using the closed-form formulas of $\tilde{\Theta}_w^l(P_m)$ in (29) and $f_{P_m}(z)$ in (21), one computes $\bar{\Theta}_w^l$ in (63) as

$$\bar{\Theta}_w^l = \int_0^\infty \tilde{\Theta}_{wl}(z) f_{P_m}(z)\,dz. \tag{65}$$

By applying a variable change $z = \tan y$, (65) is further expressed as

$$\bar{\Theta}_w^l = \int_0^{\pi/2} \tilde{\Theta}_{wl}(\tan y) f_{P_m}(\tan y)\frac{dy}{\cos^2 y}. \tag{66}$$

Utilizing Gaussian-Chebyshev quadrature in [38], (66) is strictly approximated as (28), finishing the proof.

ACKNOWLEDGMENT

The authors would like to thank the support of time and facilities from Ho Chi Minh City University of Technology (HCMUT), VNU-HCM, for this study.

REFERENCES

[1] Y. Ahn, J. Kim, S. Kim, S. Kim, and B. Shim, "Sensing and computer vision-aided mobility management for 6G millimeter and terahertz communication systems," *IEEE Trans. Commun.*, early access, Apr. 23, 2024, doi: 10.1109/TCOMM.2024.3392799.

[2] M. Shoaib, G. Husnain, N. Sayed, and S. Lim, "Unveiling the 5G frontier: Navigating challenges, applications, and measurements in channel models and implementations," *IEEE Access*, vol. 12, pp. 59533–59560, 2024.

[3] Y. Pramitarini, R. H. Y. Perdana, K. Shim, and B. An, "Opportunistic scheduling scheme to improve physical-layer security in cooperative NOMA system: Performance analysis and deep learning design," *IEEE Access*, vol. 12, pp. 58454–58472, 2024.

[4] G. S. Perera, D. Y. Senanayake, V. Basnayake, and D. N. K. Jayakody, "Dynamic spectrum fusion: An adaptive learning approach for hybrid NOMA/OMA in evolving wireless networks," in *Proc. 4th Int. Conf. Adv. Res. Comput. (ICARC)*, Belihuloya, Sri Lanka, Feb. 2024, pp. 253–258.

[5] L. Zhang, H. Yang, Y. Zhao, and J. Hu, "Joint port selection and beamforming design for fluid antenna assisted integrated data and energy transfer," *IEEE Wireless Commun. Lett.*, early access, Apr. 22, 2024, doi: 10.1109/LWC.2024.3392236.

[6] A. Essa, E. Almajali, S. Mahmoud, R. E. Amaya, S. S. Alja'Afreh, and M. Ikram, "Wireless power transfer for implantable medical devices: Impact of implantable antennas on energy harvesting," *IEEE Open J. Antennas Propag.*, vol. 5, no. 3, pp. 739–758, Jun. 2024.

[7] D. Tyrovolas, N. A. Mitsiou, T. G. Boufikos, P.-V. Mekikis, S. A. Tegos, P. D. Diamantoulakis, S. Ioannidis, C. K. Liaskos, and G. K. Karagiannidis, "Energy-aware trajectory optimization for UAV-mounted RIS and full-duplex relay," *IEEE Internet Things J.*, vol. 11, no. 13, pp. 24259–24272, Jul. 2024.

[8] H. Haritha, D. N. Amudala, R. Budhiraja, and A. K. Chaturvedi, "Superimposed versus regular pilots for hardware impaired Rician-faded cell-free massive MIMO systems," *IEEE Trans. Commun.*, early access, Apr. 23, 2024, doi: 10.1109/TCOMM.2024.3392780.

[9] Q. Li, M. El-Hajjar, Y. Sun, and L. Hanzo, "Performance analysis of reconfigurable holographic surfaces in the near-field scenario of cell-free networks under hardware impairments," *IEEE Trans. Wireless Commun.*, early access, Apr. 16, 2024, doi: 10.1109/TWC.2024.3386850.

[10] W. Zhengqiang, C. Ruifei, W. Xiaoyu, F. Zifu, and D. Bin, "Energy efficiency maximization for cooperative NOMA with hardware impairments," *China Commun.*, early access, Apr. 9, 2024, doi: 10.23919/JCC.ea.2021-0842.202401.

[11] X. Li, J. Li, and L. Li, "Performance analysis of impaired SWIPT NOMA relaying networks over imperfect Weibull channels," *IEEE Syst. J.*, vol. 14, no. 1, pp. 669–672, Mar. 2020.

[12] A. Hakimi, M. Mohammadi, Z. Mobini, and Z. Ding, "Full-duplex non-orthogonal multiple access cooperative spectrum-sharing networks with non-linear energy harvesting," *IEEE Trans. Veh. Technol.*, vol. 69, no. 10, pp. 10925–10936, Oct. 2020.

[13] C. K. Singh and P. K. Upadhyay, "Overlay cognitive IoT-based full-duplex relaying NOMA systems with hardware imperfections," *IEEE Internet Things J.*, vol. 9, no. 9, pp. 6578–6596, May 2022.

[14] K. Agrawal, M. F. Flanagan, and S. Prakriya, "NOMA with battery-assisted energy harvesting full-duplex relay," *IEEE Trans. Veh. Technol.*, vol. 69, no. 11, pp. 13952–13957, Nov. 2020.

[15] X. Lu, P. Wang, G. Li, D. Niyato, and Z. Li, "Short-packet backscatter assisted wireless-powered relaying with NOMA: Mode selection with performance estimation," *IEEE Trans. Cognit. Commun. Netw.*, vol. 8, no. 1, pp. 216–231, Mar. 2022.

[16] L. Ma, E. Li, and Q. Yang, "On the performance of full-duplex cooperative NOMA with non-linear EH," *IEEE Access*, vol. 9, pp. 145968–145976, 2021.

[17] V. Aswathi and A. V. Babu, "Outage and throughput analysis of full-duplex cooperative NOMA system with energy harvesting," *IEEE Trans. Veh. Technol.*, vol. 70, no. 11, pp. 11648–11664, Nov. 2021.

[18] K. Agrawal, A. Jee, U. Makhanpuri, and S. Prakriya, "Performance of full-duplex cooperative NOMA with mode switching and an EH near user," *IEEE Netw. Lett.*, vol. 5, no. 4, pp. 284–288, Dec. 2023.

[19] L. Tao, W. Yang, X. Lu, M. Wang, and Y. Song, "Achieving covert communication in uplink NOMA systems via energy harvesting jammer," *IEEE Commun. Lett.*, vol. 25, no. 12, pp. 3785–3789, Dec. 2021.

[20] R. Lei, D. Xu, and I. Ahmad, "Secrecy outage performance analysis of cooperative NOMA networks with SWIPT," *IEEE Wireless Commun. Lett.*, vol. 10, no. 7, pp. 1474–1478, Jul. 2021.

[21] A. Salem, L. Musavian, E. A. Jorswieck, and S. Aïssa, "Secrecy outage probability of energy-harvesting cooperative NOMA transmissions with relay selection," *IEEE Trans. Green Commun. Netw.*, vol. 4, no. 4, pp. 1130–1148, Dec. 2020.

[22] K. Cao, B. Wang, H. Ding, L. Lv, J. Tian, H. Hu, and F. Gong, "Achieving reliable and secure communications in wireless-powered NOMA systems," *IEEE Trans. Veh. Technol.*, vol. 70, no. 2, pp. 1978–1983, Feb. 2021.

[23] D. Diao, B. Wang, K. Cao, J. Weng, R. Dong, and T. Cheng, "Secure wireless-powered NOMA communications in multi-UAV systems," *IEEE Trans. Green Commun. Netw.*, vol. 7, no. 3, pp. 1205–1216, Sep. 2023.

[24] V.-H. Dang, L.-M.-D. Nguyen, V. N. Vo, H. Tran, T. D. Ho, C. So-In, and S. Sanguanpong, "Throughput optimization for noma energy harvesting cognitive radio with multi-UAV-assisted relaying under security constraints," *IEEE Trans. Cognit. Commun. Netw.*, vol. 9, no. 1, pp. 82–98, Feb. 2023.

[25] P. Yan, W. Duan, X. Ji, G. Zhang, B. Li, Y. Zou, M. Wen, and P.-H. Ho, "EH cognitive network with NOMA: Perspective on impact of passive and active eavesdropping," *IEEE Internet Things J.*, vol. 11, no. 3, pp. 5050–5062, Feb. 2024.
[26] A.-N. Nguyen, D.-B. Ha, T. V. Truong, V. N. Vo, S. Sanguanpong, and C. So-In, "Secrecy performance analysis and optimization for UAV-relay-enabled WPT and cooperative NOMA MEC in IoT networks," *IEEE Access*, vol. 11, pp. 127800–127816, 2023.
[27] K. Ho-Van, "Secure MIMO NOMA transmission with energy harvesting-aided full-duplex jammer under erroneous channel information," *Digit. Signal Process.*, vol. 151, Aug. 2024, Art. no. 104532.
[28] F. Zhao, W. Xu, and W. Xiang, "Integrated satellite-terrestrial networks with coordinated C-NOMA and relay transmission," *IEEE Syst. J.*, vol. 16, no. 4, pp. 5270–5280, Dec. 2022.
[29] F. D. Ardakani, R. Huang, and V. W. S. Wong, "Joint device pairing, reflection coefficients, and power control for NOMA backscatter systems," *IEEE Trans. Veh. Technol.*, vol. 71, no. 4, pp. 4396–4411, Apr. 2022.
[30] G. Chen, L. Qiu, and C. Ren, "On the performance of cluster-based MIMO-NOMA in multi-cell dense networks," *IEEE Trans. Commun.*, vol. 68, no. 8, pp. 4773–4787, Aug. 2020.
[31] *Study on Downlink Multiuser Superposition Transmission for LTE*, document 3GPP TR 36.859, Shanghai, China, Mar. 2015.
[32] Q. Si, M. Jin, T. A. Tsiftsis, N. Zhao, and X. Wang, "Cooperative SM-based NOMA scheme with SWIPT," *IEEE Trans. Veh. Technol.*, vol. 70, no. 6, pp. 6195–6199, Jun. 2021.
[33] Z. Ding, P. Fan, and H. V. Poor, "Impact of user pairing on 5G nonorthogonal multiple-access downlink transmissions," *IEEE Trans. Veh. Technol.*, vol. 65, no. 8, pp. 6010–6023, Aug. 2016.
[34] A. Khazali, D. Tarchi, M. G. Shayesteh, H. Kalbkhani, and A. Bozorgchenani, "Energy efficient uplink transmission in cooperative mmWave NOMA networks with wireless power transfer," *IEEE Trans. Veh. Technol.*, vol. 71, no. 1, pp. 391–405, Jan. 2022.
[35] D. Wang, F. Rezaei, and C. Tellambura, "Performance analysis and resource allocations for a WPCN with a new nonlinear energy harvester model," *IEEE Open J. Commun. Soc.*, vol. 1, pp. 1403–1424, 2020.
[36] K. Ho-Van, P. C. Sofotasios, S. Muhaidat, S. L. Cotton, S. K. Yoo, Y. A. Brychkov, O. A. Dobre, and M. Valkama, "Security improvement for energy harvesting based overlay cognitive networks with jamming-assisted full-duplex destinations," *IEEE Trans. Veh. Technol.*, vol. 70, no. 11, pp. 12232–12237, Nov. 2021.
[37] G. Cao, M. Li, H. Yuan, W. Chen, L. Li, and A. Raouf, "Error performance of RIS-assisted NOMA networks with imperfect channel state information," in *Proc. IEEE 97th Veh. Technol. Conf. (VTC-Spring)*, Jun. 2023, pp. 1–5.
[38] M. Abramowitz and I. A. Stegun, *Handbook of Mathematical Functions With Formulas, Graphs, and Mathematical Tables*, 10th ed., Washington, DC, USA: US Government Printing Office, 1972.
[39] I. S. Gradshteyn and I. M. Ryzhik, *Table of Integrals, Series and Products*, 6th ed., San Diego, CA, USA: Academic Press, 2000.
[40] S. Sesia, I. Toufik, and M. Baker, *LTE—The UMTS Long Term Evolution: From Theory to Practice*, 2nd ed., New York, NY, USA: Wiley, 2011.

TOI LE-THANH was born in Tay Ninh, Vietnam. He received the M.S. and Ph.D. degrees from Ho Chi Minh City University of Technology, Vietnam, in 2006 and 2023, respectively. Since 2003, he has been a Lecturer with Ho Chi Minh City University of Industry and Trade (HUIT), Vietnam. His research interests include wireless communications, null convention logic, asynchronous circuit design, and low power circuit design.

KHUONG HO-VAN (Member, IEEE) received the B.E. (Hons.) and M.S. degrees in electronics and telecommunications engineering from Ho Chi Minh City University of Technology, Vietnam, in 2001 and 2003, respectively, and the Ph.D. degree in electrical engineering from the University of Ulsan, South Korea, in 2007. From 2007 to 2011, he joined McGill University, Canada, as a Post-doctoral Fellow. Currently, he is an Associate Professor with Ho Chi Minh City University of Technology, Vietnam. His major research interests include modulation and coding techniques, diversity techniques, digital signal processing, energy harvesting, physical layer security, and cognitive radio.